

Learning Science Through Research

Published by the Keck Geology Consortium

Short Contributions Keck Geology Consortium Volume 36 May 2024 doi: 10.18277/AKRSG.2024.36.05

DAMAGE ZONE DEVELOPMENT AND CROSS-FAULT ASYMMETRY ON THE MT. CARMEL SEGMENT OF THE SEVIER NORMAL FAULT, SOUTHWEST UTAH

MORGAN SHARP, Whitman College

Project Advisor: Kevin Pogue

INTRODUCTION

Most fault zones are made up of a core, bounded on either side by damage zones. Damage zones are volumes of rock distinct from the fault core where the host rock is fractured at higher densities than the background level, but indicators of concentrated shear are rarely present (Fossen, 2016). Damage zones can be important conduits for subsurface fluid flow (Kim and Sanderson, 2010) and can have significant impacts on the geomorphology of fault zones (Kirkpatrick et al., 2020). Both key damage zone attributes are controlled by the characteristics of fracturing within the damage zone. Damage zones are important because of their implications for groundwater flow, hydrocarbon migration, geothermal fluid dynamics, and the evolution of topography around faults.

There are multiple models for the relationship between damage zone width and accumulation of displacement on a fault (Shipton and Cowie, 2003). One model proposes that the damage zone forms at an initial width and its width increases as displacement is accumulated on the fault (Shipton and Cowie, 2001). In another model, once the damage zone reaches maturity, its width remains relatively constant even as the fault continues to accumulate displacement (Savage and Brodsky, 2011).

A combination of ground-based scanline surveys and Structure-from-Motion (SfM) modeling was used to collect data on fracture characteristics, such as fracture spacing, orientation, and intensity, in various structural settings. The width of the damage zone was compared between locations along the fault with varying amounts of displacement. Areas where very little

displacement has been accommodated by the fault represent locations where the damage zone had less time to develop, and areas that accommodate hundreds of meters of displacement represent longer periods of damage zone development. By comparing the width of the damage zone between these two settings, the model of damage zone development which best represents the damage zones on the Sevier fault can be determined. Additionally, hanging wall fracture data was compared with footwall fracture data, which revealed asymmetries in the fracture characteristics of the two fault blocks.

BACKGROUND

The Sevier fault (called the Toroweap fault in Arizona) has a surface trace of ~ 100 km, trends N30°E, and dips to the west (e.g., Reber et al., 2001). This fault, and other large, sub-parallel normal faults are in the transition zone between the Basin and Range Province to the west and the Colorado Plateau to the east, where they accommodate extension between the two regions (Fig. 1). The Sevier fault has a maximum displacement of ~ 790 m and cuts rocks that are Precambrian to Quaternary in age (Reber et al., 2001). The recent rate of slip on the Sevier fault has been estimated at 0.018 mm/yr (Schiefelbein, 2002). The Sevier fault system is made up of numerous fault segments which meet and interact at salients, forming complex assemblages of linked faults and relay ramps (Taylor et al., in press).

The area of study was in Lower Sand Wash, a drainage where multiple segments of the Sevier fault are well-exposed just east of the town of Mt. Carmel Junction, UT. Rocks exposed in the area are primarily of the Jurassic Navajo Sandstone, which is aeolian in origin.

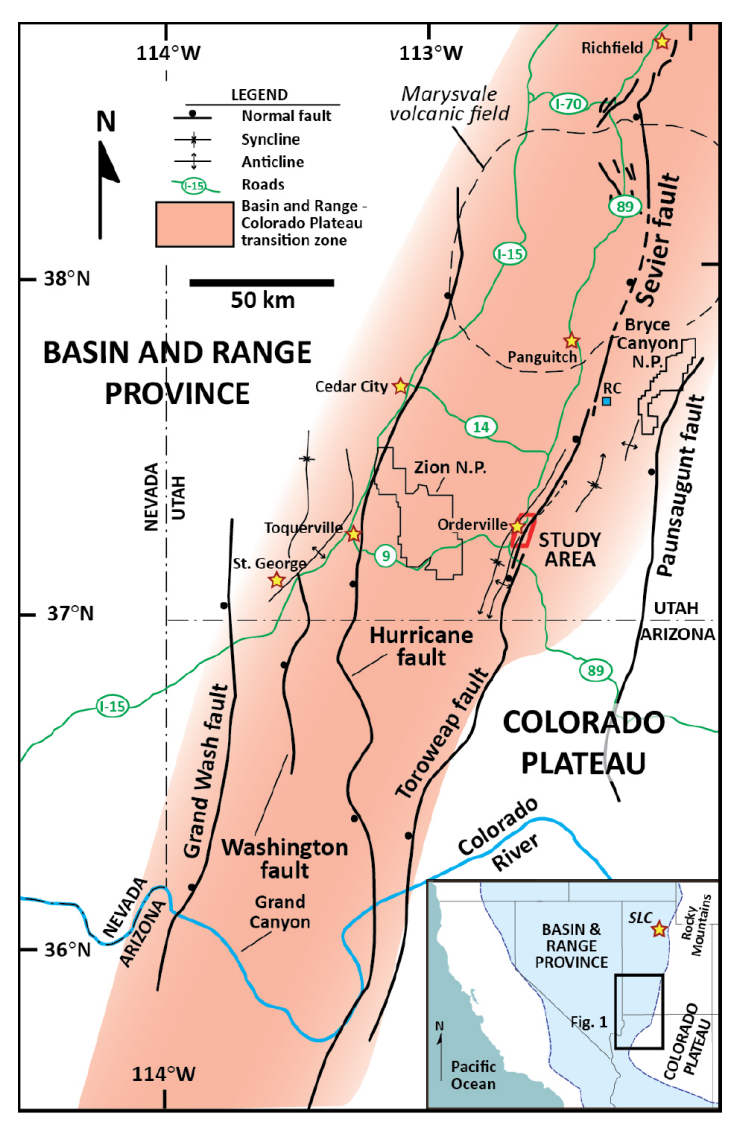


Figure 1. Overview map of the Basin and Range-Colorado Plateau transition zone showing the major faults that accommodate extension in the area. See inset for regional location of main figure map. Note the location of the study area denoted by the red box to the east of the community of Orderville. Ball symbols are on the hanging wall side of fault traces. Figure is modified from Taylor et al., in press.

Lower Sand Wash was selected due to its wellexposed bedrock outcrops as well as its accessibility for ground-based surveys.

METHODS

Field Methods

On well-exposed and continuous outcrops, scanlines were established perpendicular to the dominant fracture plane orientation, and the dip and dip direction of each continuous fracture on the scanline was measured along with the spacing between

fractures (Fig. 2). The positions of scanline start and end points and other locations of interest (fault plane exposures, slickenline exposures, etc.) were recorded with a Trimble Geo XH handheld global positioning system receiver (30 cm accuracy). Location data were compiled in a GIS database. Scanline measurements were complimented by field photographs, descriptions, and detailed sketches of important structural features.

A DJI Phantom 4 drone was flown along the Mt. Carmel fault segment and adjacent areas to record high resolution video of the land surface. Flights were conducted during the midday hours for improved contrast and image quality. UAV surveys provided imagery of areas such as canyon walls, cliff faces, and remote uplands which were inaccessible on foot.

3D Model Construction

VLC Media Player was used to extract still images from UAV-captured video at a rate of one image per second, providing the image-to-image overlap needed for model construction. Images were imported into Agisoft Metashape Professional version 2 (Agisoft) to construct spatially accurate, georeferenced Structure from Motion (SfM) models of the land surface. In



Figure 2. Geologists measuring the attitude of and spacing between fractures along a scanline in Lower Sand Wash.

Agisoft, images were aligned, and a point cloud, mesh and model texture were built. Models were georeferenced by selecting identifiable ground control points (GCPs) in Google Earth Pro and placing markers on corresponding points on the models using Agisoft's georeferencing tool. Finally, map view orthomosaics of georeferenced models were generated in Agisoft.

Fracture Mapping and Analysis

Agisoft's markup tools were used to annotate all fractures visible in the orthomosaic. Once fractures were annotated, scanlines were established perpendicular to the dominant fracture orientation (strike) on well-exposed outcrops and spacing between fractures was measured.

For all scanlines, both model-based and field-based, fracture intensity was calculated as the number of fractures per meter along the scanline. The regularity of fracture spacing was calculated using Cv', defined as Cv' = σ / M, where σ = the standard deviation of fracture spacings in a scanline and M = the median fracture spacing in the scanline. Cv' = 1 is the cutoff above which fracture spacing is more clustered than random and below which it is more regular than random (Hooker et al., 2023). Stereonet plots of fracture orientations were also created from scanline data.

The width of the damage zone was measured using aerial imagery to make a visual estimate of where fracturing reduced to background levels. Footwall and hanging wall damage zone widths were measured at Lower Sand Wash, and footwall width was measured at the location of maximum displacement on the Mt. Carmel segment, ~ 3 km north of Lower Sand Wash.

RESULTS

Footwall damage zone width measurements in the Jurassic Navajo Sandstone show that at the point of maximum displacement along strike of the Mt. Carmel fault segment (Surpless, unpub.), throw is \sim 790 m and the footwall damage zone is \sim 54 m wide. In Lower Sand Wash, throw is \sim 150-220 m and the footwall damage zone is \sim 44 m wide. The hanging wall damage zone width in Lower Sand Wash is \sim 102

m (Fig. 3).

Fractures in the footwall generally fall into a wideranging set with strikes ranging from $\sim 330^\circ$ to $\sim 30^\circ$ (Fig. 4). The 30° end of this range is roughly parallel to the main strand of the Mt. Carmel fault segment in this location, while the 330° end of the range aligns with the prominent gullies cutting into the footwall (two are visible in Figure 4). Fractures in the hanging wall cluster into two dominant sets (Fig. 4). One has strikes ranging from $\sim 260^\circ$ to $\sim 330^\circ$ and is roughly perpendicular to the strike of the fault. The other set has strikes ranging from $\sim 30^\circ$ to $\sim 60^\circ$ and is roughly fault-parallel.

Cv' and fracture intensity data plots show no clear trends separating values in the hanging wall and the footwall (Fig. 5). Footwall scanlines have a Cv' range of 0.76 - 3.41 and a fracture intensity range of 0.57 - 2.45 fractures / meter. Hanging wall scanlines have a Cv' range of 0.73 - 4.12 and a fracture intensity range of 1.18 - 3.83 fractures / meter.

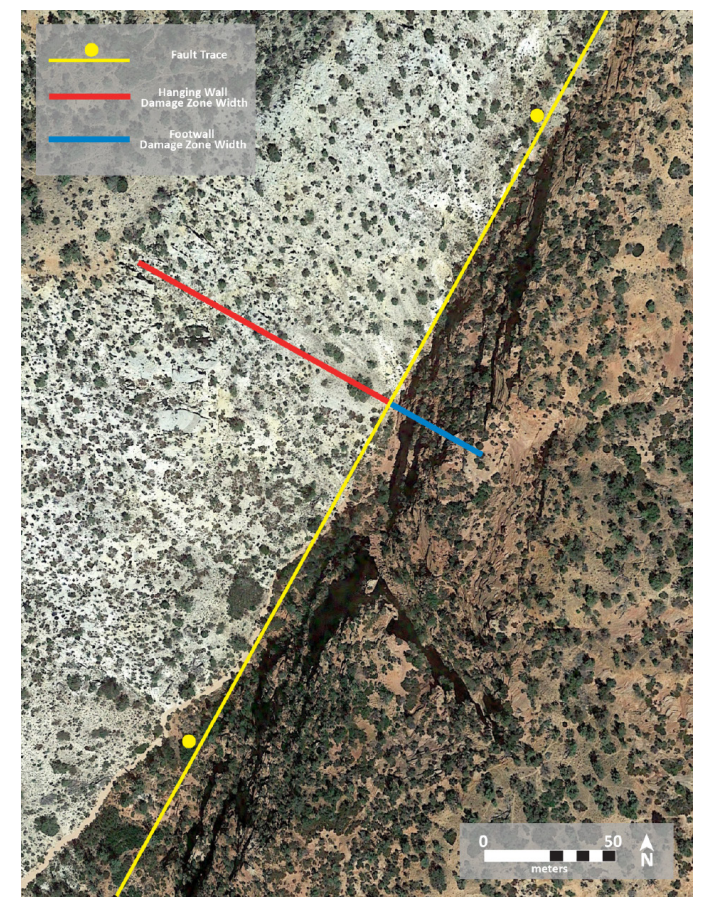


Figure 3. Detail map of the upper canyon in Lower Sand Wash annotated with the fault trace as well as the measured widths of the damage zones in the footwall (blue) and hanging wall (red). Ball symbols are on the hanging wall side of the fault trace.

DISCUSSION

Damage Zone Width Across Displacements

The fact that footwall damage zone width varies only on the meter scale over a range of displacements that vary on the scale of hundreds of meters suggests that a simple scaling model cannot be used to explain the relationship between footwall damage zone width and displacement. The constant width model is likely a more accurate representation of the damage zone width development style occurring on the Mt. Carmel segment of the Sevier fault.

Savage and Brodsky (2011) divide the "lifespan" of a normal fault into two phases: in the first, damage zone width increases proportionally to displacement on the fault, and in the second, at displacements greater than ~150 m, damage zone width increase slows and

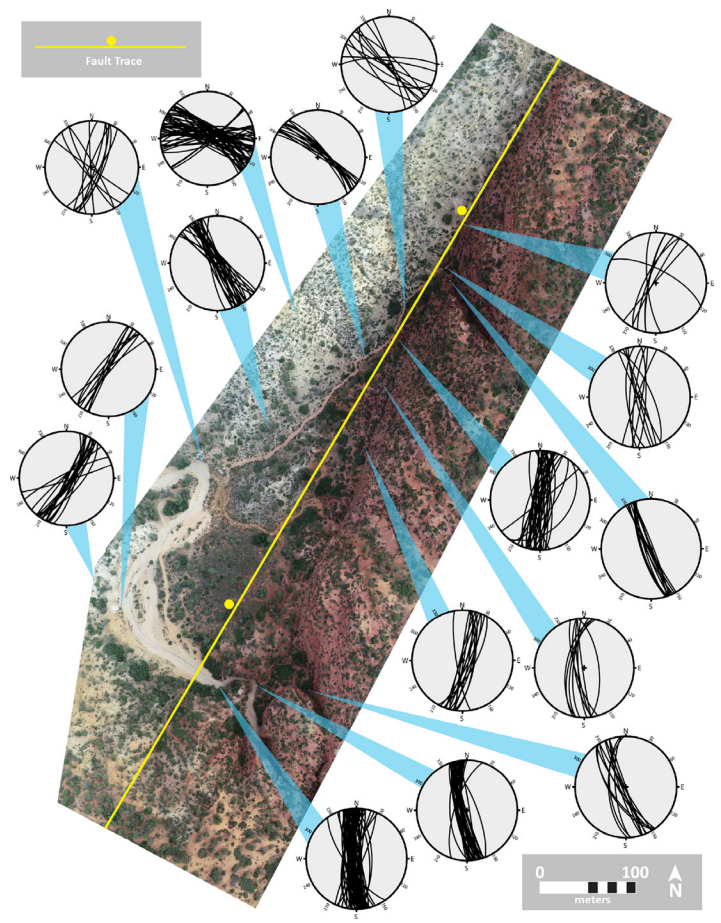


Figure 4. Orthomosaic of Lower Sand Wash annotated with the fault trace and stereonets showing the fracture orientations of each scanline and where each scanline was measured in the field. Stereonets representing scanlines measured in the footwall are displayed to the right of the orthomosaic and those representing scanlines measured in the hanging wall are displayed to the left. Ball symbols are on the hanging wall side of the fault trace.

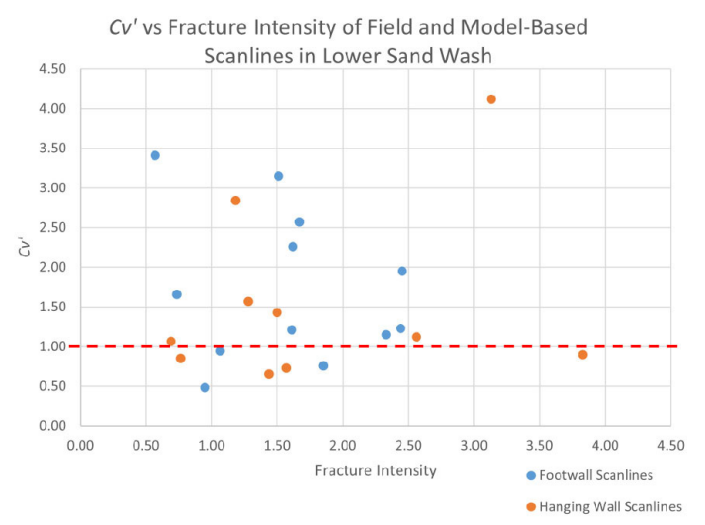


Figure 5. Scatter plot of the Cv' and fracture intensity values of field-based as well as model-based scanlines in Lower Sand Wash, with fracture intensity on the x-axis and Cv' on the y-axis. Scanlines measured in the footwall are represented by blue points and those measured in the hanging wall are represented by orange points. The red dashed line represents the cutoff (Cv' = 1) above which fracture spacing is more clustered than random.

is not strongly tied to displacement accumulation. At both locations where footwall damage zone width was measured, displacements were greater than ~150 m, thus the displacement and displacement-damage zone width relationship observed at these two locations align with Savage and Brodsky's (2011) descriptions of the second phase of a fault's "lifespan" in which displacement accumulation and damage zone width are not strongly related.

Asymmetry Between Fault Blocks

Fracture orientation data show asymmetry between the hanging wall and footwall. While the set of roughly fault-parallel fractures striking ~ 30° is present in both the footwall and the hanging wall (Fig. 4), the scanlines in the hanging wall that contain this fracture set are farther from the fault and closer to a secondary fault strand than the other hanging wall scanlines. Due to their proximity to the secondary fault strand, these fault-parallel fractures may be formed by stresses in the footwall of the secondary strand. If this is the case, this fracture set fits into the overall trend shown in the data, with roughly fault-parallel fractures in the footwall and roughly fault-perpendicular fractures in the hanging wall. Strain modeling done on the Sevier fault by Jennings (2024) also found fracture orientation asymmetries between fault blocks. In their modeling, the same footwall-hanging wall fracture

orientation trend occurs at 3 km depth (Jennings, 2024). This suggests that the rock presently exposed at the surface may have been at a significant depth at the time of faulting.

Cross-fault asymmetry in damage zone width has been documented in normal fault systems by previous studies (Berg and Skar, 2005; Liao et al., 2020). Berg and Skar (2005) favor an asymmetrical stress field as the primary control on this asymmetry. Differing lithology in the two fault blocks due to fault-offset is another potential control on asymmetrical damage zone characteristics. In the case of Lower Sand Wash, the Navajo Sandstone is exposed in both the hanging wall and the footwall, so cross-fault lithological variation is not likely a significant control on these asymmetries.

Cv' and fracture intensity data do not reveal cross-fault asymmetries (Fig. 5). Given the asymmetries shown in the other cross-fault datasets, either 1) the factors controlling the observed asymmetries do not impact fracture clustering and intensity or 2) the collected fracture clustering and intensity data are insufficient to reflect these asymmetries due to small sample size or topographic relief limitations on data collection.

CONCLUSIONS

Analysis of scanline and SfM data from the Mt. Carmel segment of the Sevier fault in southwest Utah supports a "constant width" model of damage zone development and displays distinct asymmetries between the hanging wall and footwall.

Observations of damage zones in the footwall show very similar widths (\sim 44 m and \sim 54 m) across a wide range of fault displacements (\sim 150 m to \sim 790 m). This suggests that damage zone development in Lower Sand Wash is better represented by a "constant width" model – in which damage zone width is not strongly controlled by displacement – than a scaling model.

Differing fracture orientations and damage zone widths in the hanging wall and footwall suggest asymmetries in strain between the two fault blocks. Specifically, the footwall is dominated by fault-parallel fractures, the hanging wall is dominated by fault-perpendicular fractures, and the hanging wall

damage zone is more than two times wider than that of the footwall. The data do not show asymmetries in fracture intensity or clustering between the two fault blocks.

ACKNOWLEDGEMENTS

This material is based upon work supported by the Keck Geology Consortium and the National Science Foundation under Grant No. 2050697. Funding was also provided by NSF Award 2042114 to PI Surpless and by the Trinity University Department of Geosciences. Thank you to my advisors, Drs. Ben Surpless and Kevin Pogue for their guidance and feedback. Thanks also to the field crew: Audrey, Demi, Pierce, and Jack.

REFERENCES

Fossen, H., 2016, Structural Geology: Cambridge, England, Cambridge University Press.

Hooker, J.N., Marrett, R., and Wang, Q., 2023, Rigorizing the use of the coefficient of variation to diagnose fracture periodicity and clustering: Journal of structural geology, v. 168, p. 104830, doi:10.1016/j.jsg.2023.104830.

Jennings, A., 2024, Computer Modeling of Normal Fault-Related Damage Zones: Implications for Estimating Geothermal Energy Potential: Trinity University B.S. Thesis, 63 p.

Kim, Y.-S., and Sanderson, D.J., 2010, Inferred fluid flow through fault damage zones based on the observation of stalactites in carbonate caves: Journal of structural geology, v. 32, p. 1305–1316, doi:10.1016/j.jsg.2009.04.017.

Kirkpatrick, H.M., Moon, S., Yin, A., and Harrison, T.M., 2020, Impact of fault damage on eastern Tibet topography: Geology, v. 49, p. 30–34, doi:10.1130/G48179.1.

Liao, Z., Hu, L., Huang, X., Carpenter, B.M., Marfurt, K.J., Vasileva, S., and Zhou, Y., 2020, Characterizing damage zones of normal faults using seismic variance in the Wangxuzhuang oilfield, China: Interpretations v. 8, p. 1-24.

Reber, S., Taylor, W.J., Stewart, M., and Schiefelbein, I.M., 2001, Linkage and reactivation along the northern Hurricane and Sevier faults, southwestern Utah: Utah Geological Association

- Publication 30 and Pacific Section American Association of Petroleum Geologists Guidebook GB 78, p. 379-400.
- Savage, H.M., and Brodsky, E.E., 2011, Collateral damage: Evolution with displacement of fracture distribution and secondary fault strands in fault damage zones: Journal of geophysical research, v. 116, doi:10.1029/2010jb007665.
- Schiefelbein, I., 2002, Fault segmentation, fault linkage, and hazards along the Sevier Fault, southwestern Utah [M.S. thesis]: Las Vegas, University of Nevada.
- Shipton, Z.K., and Cowie, P.A., 2003, A conceptual model for the origin of fault damage zone structures in high-porosity sandstone: Journal of structural geology, v. 25, p. 333–344, doi:10.1016/s0191-8141(02)00037-8.
- Shipton, Z.K., and Cowie, P.A., 2001, Damage zone and slip-surface evolution over μm to km scales in high-porosity Navajo sandstone, Utah: Journal of structural geology, v. 23, p. 1825–1844, doi:10.1016/s0191-8141(01)00035-9.
- Surpless, B., unpublished, Geologic cross-section of the Mt. Carmel segment of the Sevier fault zone, southern Utah.
- Taylor, W., Surpless, B., and Schiefelbein, I., 2024, Complex segment linkage along the Sevier normal fault, southwestern Utah: Geosphere (in press).